AIAA JOURNAL
Vol. 35, No. 3, March 1997

Optimum Design and Validation of Flat Composite Beams Subject to Frequency Constraints

J. M. Taylor* and R. Butler†
University of Bath, BA2 7AY Bath, England, United Kingdom

The use of the dynamic stiffness method has been extended to permit optimum (minimum mass) design of nonuniform composite beams subject to frequency constraints. The beams are modeled as a series of elements, stepped in thickness at discrete nodes, and are constrained to have a minimum separation between first bending and first torsional frequencies. The frequency constraints are supplied to the optimizer, DOT (design optimization tools), using the dynamic stiffness method, which incorporates a mode tracking routine to ensure that the first bending and first torsional natural frequencies are located at each design iteration. An optimum design has been manufactured from a carbon fiber/epoxy composite and subjected to an experimental modal analysis to validate the results. The dynamic stiffness method has a maximum difference of 11% from the experimentally obtained natural frequencies. In addition, a finite element model of the optimum design has been developed and showed a maximum difference of 13% from the experimental results. Analysis using the dynamic stiffness method is as accurate, much faster (in excess of 2 orders of magnitude), and considerably simpler than the finite element method for this type of problem.

I. Introduction

MUCH research has been conducted into the use of material bending–torsion coupling to optimize the free vibration characteristics of composite beams. In particular, the potential to maximize the speed at which an aircraft wing undergoes classic flutter and divergence has received notable attention. Such aeroelastic tailoring, as well as structural optimization subject to frequency constraints, has been well documented in review papers by Shirk et al.[1] and Grandhi,[2] respectively.

The benefits of using composites in place of metallic materials for frequency-constrained optimization are due to their directional stiffness and strength properties, their high stiffness-to-weight ratio, and the ability to couple bending and torsional displacements. Together, these features allow a latitude in design that is not available with conventional metals. The effect of coupled bending–torsional rigidity on the free-vibration node line position and frequencies of a cantilever beam was examined by Weisshaar and Foist.[3] A finite element method (FEM) was used to show that the amount of coupling has a significant effect on both the mode shapes and the frequencies. In addition, Hollowell and Dugundgji[4] conducted detailed investigations into varying such coupling in composite uniform flat plates to ascertain the effect this has on divergence and flutter onset. Their tests gave natural frequency results and included detailed low-speed wind-tunnel analysis. Also, parametric studies, which examine the effect that fiber orientation of composite layers within a (uniform) laminated beam have on flutter speed, have been presented by a number of authors (for example, see Ref. 5). These recommend that for aft swept composite wings, the coupled bending–torsional rigidity should be negative to maximize the flutter speed [i.e., when air flows in the negative x direction, the laminate should have a greater number of plies with negative ply angle than positive (see Fig. 1), where θ (ply angle) is defined positive as shown]. Finally, Meirovitch and Seitz[6] have recently combined frequency-constrained structural optimization with aeroelastic tailoring and studied the structural modeling of low aspect ratio composite wings. Particular attention was paid to the pitch and plunge rigid body degrees of freedom.

There also have been a number of methods developed to undertake the optimization of both metallic and composite wing structures. In 1992, Grandhi et al.[7] utilized a generalized compound scaling algorithm in the optimum design of plate structures with frequency constraints. This treated the objective function as an additional constraint given that both the original constraints and the objective function are functions of the same variables. In addition, Butler and Banerjee[8] have recently developed a procedure for optimum (mimimum mass) design of nonuniform metallic beams subject to frequency constraints using the dynamic stiffness method (DSM). Compared with the FEM, which gives a solution in which accuracy is dependent on the number of degrees of freedom, the DSM involves the exact solution of the governing equations of motion allowing all natural frequencies to be found to any desired accuracy. The method also requires few degrees of freedom and is therefore extremely efficient, which is particularly important for optimization. However, the method is not as general as the FEM, which may be applied to fully three-dimensional structures, but is ideal for structures that may be modeled as nonuniform beams or prismatic plate assemblies.

This paper extends the use of the DSM to enable minimum mass optimization of nonuniform composite beams subject to frequency constraints. The optimization program that has been developed considers layer thickness as design variables given a generic layup and utilizes the method of feasible directions to calculate each new design iteration. An optimum design produced by the program is manufactured from a carbon fiber/epoxy composite and is then validated by experimental modal analysis. Finally, the frequencies obtained are compared to the results of modeling the optimum design by using the commercial FEM package ANSYS.[9]

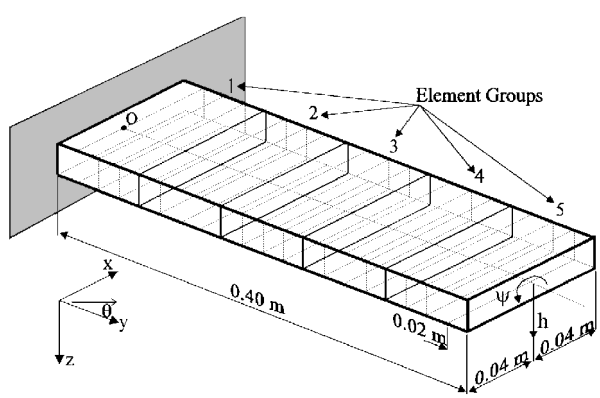

Fig. 1 Coordinate system, notation, and elemental setup of composite beam (where θ is ply angle).

Received Feb. 22, 1996; revision received Aug. 5, 1996; accepted for publication Nov. 29, 1996; also published in *AIAA Journal on Disc*, Volume 2, Number 2.

*Research Student, School of Mechanical Engineering.
†Lecturer, School of Mechanical Engineering.

II. Theory

A. Structural Model

Composite beams are modeled as series of uniform, connected elements cantilevered at the root, and each element obeys the following relationships between force and displacement:

$$M = -EI\frac{\partial^2 h}{\partial y^2} - K\frac{\partial \psi}{\partial y} \tag{1}$$

$$T = GJ\frac{\partial \psi}{\partial y} + K\frac{\partial^2 h}{\partial y^2} \tag{2}$$

where M is the bending moment, T is the torque, h is the vertical displacement, ψ is the torsional displacement, and y is the length along the beam (see Figs. 1 and 2). EI, GJ, and K, which are constant for each element, are the flexural rigidity, torsional rigidity, and coupled bending–torsional rigidity, respectively.

The rigidity properties described are derived from the anisotropic plate and laminate theory found in Refs. 10 and 11. The relationship between plate bending moments, torsional moments, and curvatures of the midsurface of a plate can be expressed as

$$\begin{Bmatrix} M_x \\ M_y \\ M_{xy} \end{Bmatrix} = \begin{bmatrix} D_{11} & D_{12} & D_{16} \\ D_{12} & D_{22} & D_{26} \\ D_{16} & D_{26} & D_{66} \end{bmatrix} \begin{Bmatrix} k_x \\ k_y \\ k_{xy} \end{Bmatrix} \tag{3}$$

where the elements $D_{ij}(i, j = 1, 2, 6)$ are the flexural modulus components of a laminated composite plate that depends on both the fiber orientation and the stacking sequence of the individual plies in the lamina.

If the y axis shown in Fig. 1 is taken as the reference axis, then the plate deflection $w(x, y)$, the beam deflection $h(y)$, and twist $\psi(y)$ are defined as

$$h(y) = w(0, y) \tag{4}$$

$$\frac{\partial w}{\partial x}_{x=0} = -\psi(y) \tag{5}$$

Thus, in this case, the plate curvatures may be approximated as

$$k_y \approx -\frac{\partial^2 h}{\partial y^2} \tag{6}$$

$$k_{xy} \approx 2\frac{\partial^2 w}{\partial x \partial y}_{x=0} = -2\frac{\partial \psi}{\partial y} \tag{7}$$

The relationships between moment resultants on the beam and those on the plate cross-section, as seen in Ref. 10, are found to be

$$M = -bM_y \tag{8}$$

$$T = 2bM_{xy} \tag{9}$$

where b is the width of the plate. If the chordwise moment M_x is assumed to be zero, then the effective bending, torsional, and coupling rigidities (EI, GJ, and K, respectively) can be expressed in terms of the plate properties in Eq. (3) as follows (for example, see Ref. 3):

$$EI = b\left[D_{22} - (D_{12}^2/D_{11})\right] \tag{10}$$

$$GJ = 4b\left[D_{66} - (D_{16}^2/D_{11})\right] \tag{11}$$

$$K = 2b\left[D_{26} - \frac{D_{12}D_{16}}{D_{11}}\right] \tag{12}$$

The rigidity properties derived above are used in the free vibration analysis below.

B. Free Vibration Analysis

The DSM for composite beams involves assembly of a single, frequency-dependent stiffness matrix, the elements of which are transcendental functions of both mass and stiffness terms. The method produces an exact solution in the sense that the dynamic stiffness matrix is obtained from the exact solution of the governing differential equations of motion for the structural element. Consequently, the only assumptions made are those associated with how the motion of the element is described by the differential equations. The main difference between this and more traditional finite element approaches is that in the latter the mass and stiffness matrices are obtained separately and the former essentially assumes a continuous distribution of stiffness and mass over the structure, thus allowing for an infinite number of degrees of freedom. In contrast, the FEM discretizes the stiffness and the mass distribution onto nodal points and uses a finite number of degrees of freedom. Hence, they can find only the same finite number of modes as the number of degrees of freedom used to model the problem, with inaccuracy increasing for the higher modes found. However, because of the simplicity of the structural elements that may be used by the DSM compared with those that may be used in the FEM, the latter is much more capable of detailed analysis of complex structures. The method is, however, suitable for the conceptual/preliminary design of structures that may be modeled as nonuniform beams, e.g., high-aspect-ratio aircraft wings.

For the beam elements considered here, the dynamic stiffness matrix is formed from the exact solution of the following two differential equations:

$$EI\frac{\partial^4 h}{\partial y^4} + K\frac{\partial^3 \psi}{\partial y^3} + m\frac{\partial^2 h}{\partial t^2} = 0 \tag{13}$$

$$GJ\frac{\partial^2 \psi}{\partial y^2} + K\frac{\partial^3 h}{\partial y^3} - I_P\frac{\partial^2 \psi}{\partial t^2} = 0 \tag{14}$$

where t is time and m and I_P, which are constant for each element, are the mass per unit length and the polar mass moment of inertia per unit length, respectively. Note that the effects of rotary inertia, shear deformation, and warping stiffness are considered to be small and are thus neglected in these equations.

In deriving the dynamic stiffness matrix, the vertical and torsional displacements (h and ψ) are given sinusoidal variations in time, so that

$$h(y, t) = H(y)\sin\omega t \tag{15}$$

$$\psi(y, t) = \Psi(y)\sin\omega t \tag{16}$$

where ω is circular frequency and the solutions for Ψ and H, which are the nodal amplitudes of ψ and h, are obtained in terms of a set of arbitrary constants. These constants are then eliminated by imposing the prescribed end conditions (see Fig. 2) for the beam displacements (H_1, Θ_1, and Ψ_1 and H_2, Θ_2, and Ψ_2) and forces (S_1, M_1, and T_1 and S_2, M_2, and T_2). Reference 12 contains full details of this procedure. The natural frequencies (eigenvalues) of the elements may then be found by solving the following equation:

$$[K(\omega)]\{D\} = \{0\} \tag{17}$$

where $\{D\}$ is the vector of nodal amplitudes H, Θ, and Ψ, and $[K(\omega)]$ is the dynamic stiffness matrix, the elements of which are transcendental functions of frequency. The algorithm developed by Wittrick and Williams[13] is used to ensure that any desired natural

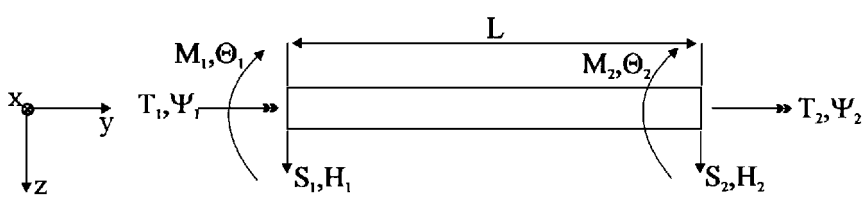

Fig. 2 End conditions for forces and displacements of a beam element of length *L*.

frequency is found both with certainty and exactly, i.e., to the accuracy specified in the program. (A relative accuracy of 10^{-5} is used in Sec. III.)

C. Optimization

The optimization procedure utilizes the method of modified feasible directions contained within the Fortran program DOT (design optimization tools)[14] to iteratively apply design variable changes to the following constrained problem:

$$\text{minimize } W \tag{18}$$

$$\text{subject to } G_n \leq 0 \qquad n = 1, 2, 3, \ldots, n_c \tag{19}$$

$$\text{and } \{X_L\} \leq \{X\} \leq \{X_U\} \tag{20}$$

where W, the mass of the beam, is the objective function, G_n are the n_c frequency constraints, and $\{X_L\}$ and $\{X_U\}$ are the lower and upper bounds, respectively, on the design variables $\{X\}$. W and G_n are both functions of $\{X\}$. The modified method of feasible directions is a gradient search technique, which requires calculation of the sensitivity of G_n and W to design variable changes to find a "usable–feasible" direction in which to move the design. (A usable direction is one that moves the design closer to the optimum; a feasible direction ensures that this move does not violate one or more of the design constraints.)

The constraint evaluations for each design iteration are carried out by the analysis method described above. The constraint used in this paper specifies a lower limit on the difference ω_{diff}, prescribed in the data input, between some frequency ω_i and some higher frequency ω_h, where

$$G_n = 1 - \frac{\omega_h - \omega_i}{\omega_{\text{diff}}} \qquad \text{for} \quad h > i \tag{21}$$

Given the transcendental nature of the eigenvalue problem, the sensitivity of constraints to design variable changes is found by using a numerical forward finite difference scheme with a step size of 0.001. A constraint is considered active if its value is more positive than -0.03 and violated if it is greater than $+0.003$. Convergence occurs when, for two consecutive design iterations, the relative change in W is less than 0.1%.

III. Results and Discussion

A. Frequency Optimization of Nonuniform Composite Beams

The initial design used here consisted of a uniform beam made up of 20 similar elements of layup $[90/0/-45/+45]_s$ with overall dimensions given in Fig. 1 and material properties given in Table 1. Symmetry of the layup was maintained throughout optimization and the thickness of each of the 90-, 0-, -45-, and $+45$-deg layers was allowed to vary within the limits of 0.125 mm (a single ply of prepreg material) and 2.0 mm (16 plies). For ease of manufacture, the beam was divided into five element groups (see Fig. 1), and the thickness of the layers within each group was kept constant. Varying the thickness of the four plies in the five element groups resulted in a total of 20 design variables. Initially, each of the eight layers was made up of four plies, i.e., $[90_4/0_4/-45_4/+45_4]_s$, where each ply was 0.125 mm thick, giving an initial beam thickness of 4.0 mm. The first bending and first torsional frequencies for the starting design were 156.30 and 956.54 rad/s, respectively. The frequency constraints imposed on the optimization process took the form of Eq. (21), so that the mass of the design, W, was minimized, whereas separation between the natural frequencies corresponding to the first bending mode and the first torsional mode was constrained to be greater than or equal to some specified value, ω_{diff}. This is generally recognized as being good design practice from the aspect of avoiding classic wing flutter, which involves the coalescence of bending and torsional modes as a function of airspeed. To ensure that at each iteration the constraint was calculated from the correct frequencies, the optimization code contained a mode tracking routine. Here, each mode shape was found by calculating $\{D\}$ in Eq. (17) for each ascending natural frequency and normalizing each $\{D\}$ with respect to the largest value of H, Θ, and Ψ. The first mode to have a value of H or Θ as its largest nodal amplitude was assumed to be first bending, and the first mode to have a value of Ψ as its largest nodal amplitude was assumed to be first torsion. This method was used to indicate the first bending and first torsional modes throughout optimization.

Table 1 Material properties of Cytek 5245-T800 carbon fiber/epoxy composite

Parameter	Value
E_1	165.0 GPa
E_2	8.8 GPa
G_{12}	5.0 GPa
G_{13}	5.0 GPa
G_{23}	2.5 GPa
ν_{12}	0.30
ρ	1550 kg/m^3

The values of ω_{diff} used for optimization were 550, 650, 750, 850, and 950 rad/s, producing five different optimum designs. The progress of the objective, normalized with respect to the optimum mass W_{opt}, and constraint (G_1) during the optimization process for an ω_{diff} of 750 rad/s is shown in Fig. 3. It can be seen that the optimizer attempts to satisfy the constraint in the first iteration with little concern for the effect on mass. Subsequent iterations then proceed to reduce the objective while keeping the frequency constraint satisfied given the tolerances used by DOT.

Figure 4 shows the variation in thickness of the -45- and $+45$-deg layers that takes place in each of the groups of elements 1

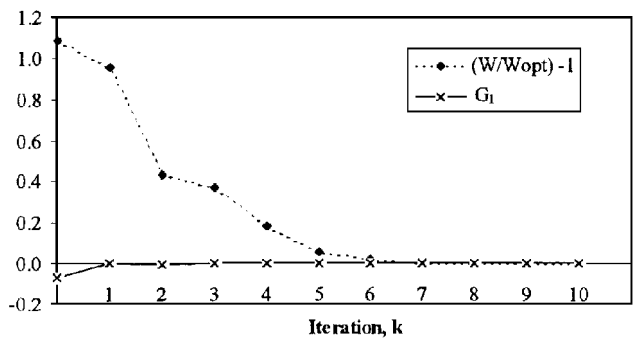

Fig. 3 Constraint and objective progress during optimization (ω_{diff} = 750 rad/s).

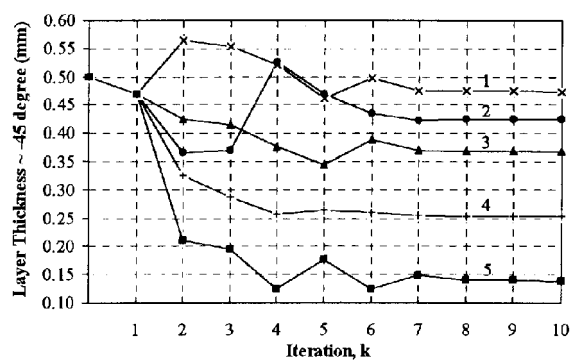

a) -45-deg layers

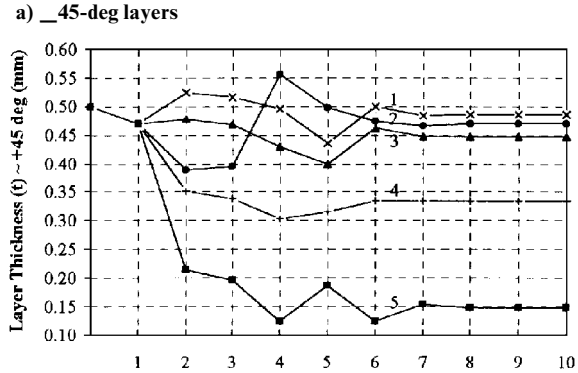

b) + 45-deg layers

Fig. 4 Design variable history (ω_{diff} = 750 rad/s). Numbers on plots indicate element groups.

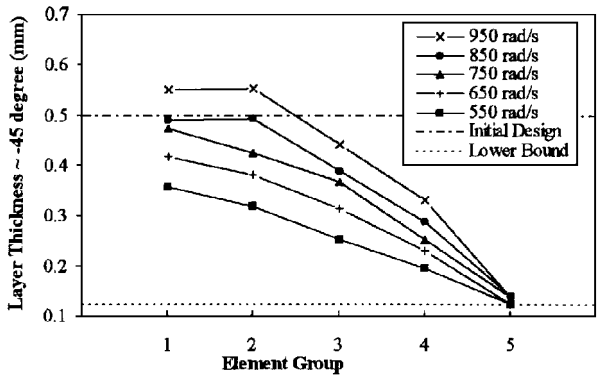

a) _45-deg layer thickness

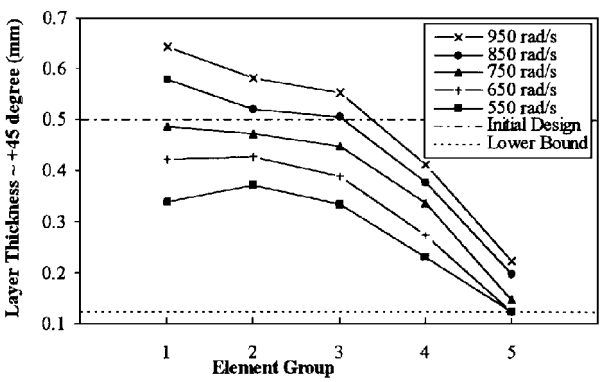

b) + 45-deg layer thickness

Fig. 5 Variation for optimum beam designs with different values of frequency separation ω_{diff}.

(root) to 5 (tip) over the course of the optimization. The results shown are for a frequency separation of 750 rad/s. Similar plots of the 90- and 0-deg fibers are not shown, as by iteration 7 both of these layers are at their minimum allowable thickness of 0.125 mm. The thicknesses of _45- and +45-deg layers are initially decreased throughout the beam to capture the frequency constraint before the beam is optimized to achieve its final tapered form.

In Fig. 5, the thicknesses of _45- and +45-deg layers for optimum designs for the range of ω_{diff} considered are displayed to illustrate the design trends for separating first bending and first torsional frequencies. Similar plots of 90- and 0-deg layers are not shown as these layers are reduced to their lower bound of 0.125 mm, i.e., single-ply thickness, throughout. As shown, beam mass is reduced by decreasing layer thickness toward the tip. In addition, this has the effect of reducing I_p and m, which, respectively, increase the torsional frequency and bending frequency, with the former effect being more pronounced. Increasing layer thickness toward the root has a similar effect on EI and GJ and in turn increases the bending and torsional frequencies. Once again, the effect on torsional frequency is more pronounced.

Variations of EI, GJ, and K are plotted in Fig. 6. The graphs display a smooth decrease in the values of bending rigidity, torsional rigidity, and bending–torsion coupling from root to tip for all values of ω_{diff}. The value of EI for the initial design was 25.63 Nm^2, which is considerably higher than the optimized result; K, the coupled bending-torsional rigidity, and GJ, the torsional rigidity, are closer to their initial design values. The effect of K was investigated by putting K equal to zero for the $\omega_{\text{diff}} = 750$ rad/s optimum design. This reduced the first bending frequency from 125.2 to 33.6 rad/s and reduced the first torsional frequency from 917.5 to 259.3 rad/s.

Finally, Fig. 7 shows the relationship between optimum mass and the first bending and the first torsional frequencies for the five designs considered. For the range of frequency separations covered, optimum mass increases fairly linearly with increasing ω_{diff}.

B. Experimental Methodology

To validate the program, the optimum design having an ω_{diff} of 750 rad/s was manufactured from a carbon fiber/epoxy composite.

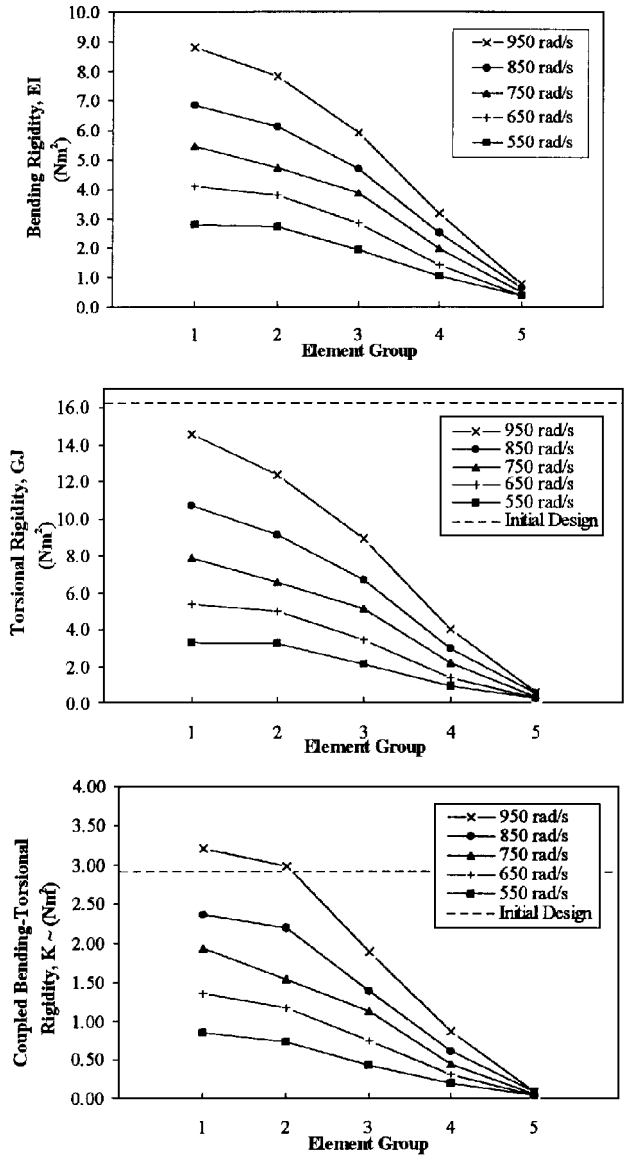

Fig. 6 Variation of rigidities for optimum beam designs with different values of frequency separation ω_{diff}.

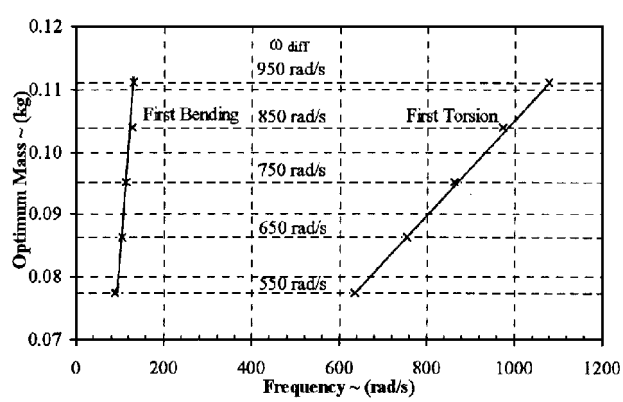

Fig. 7 Optimum design mass against first bending and first torsional natural frequencies for composite beams.

To make this possible, the optimum obtained earlier was subject to the discrete optimization routine within DOT. Here, DOT treated the continuous solution as a lower limit and then used a "branch and bound" method to select the nearest thickness that corresponded to a whole number of plies (see Ref. 14). This gave the discrete solution shown in Table 2. During the discretization routine, the optimum mass increased from 0.0951 to 0.0967 kg, but the frequency constraint remained satisfied.

Table 2 Continuous and discrete optimization results for ω_{diff} = 750 rad/s

Element group	Continuous optimum t_{90}, mm $\times 10^{-3}$	t_0, mm $\times 10^{-3}$	t_{-45}, mm $\times 10^{-3}$	t_{+45}, mm $\times 10^{-3}$	Discretized optimum
1	0.125	0.125	0.462	0.500	$[90/0/\_45_4/+45_4]_s$
2	0.125	0.125	0.438	0.479	$[90/0/\_45_4/+45_4]_s$
3	0.125	0.125	0.368	0.425	$[90/0/\_45_3/+45_3]_s$
4	0.125	0.125	0.261	0.336	$[90/0/\_45_2/+45_3]_s$
5	0.125	0.125	0.137	0.139	$[90/0/\_45/+45]_s$
Total mass, W	0.095 kg				0.097 kg

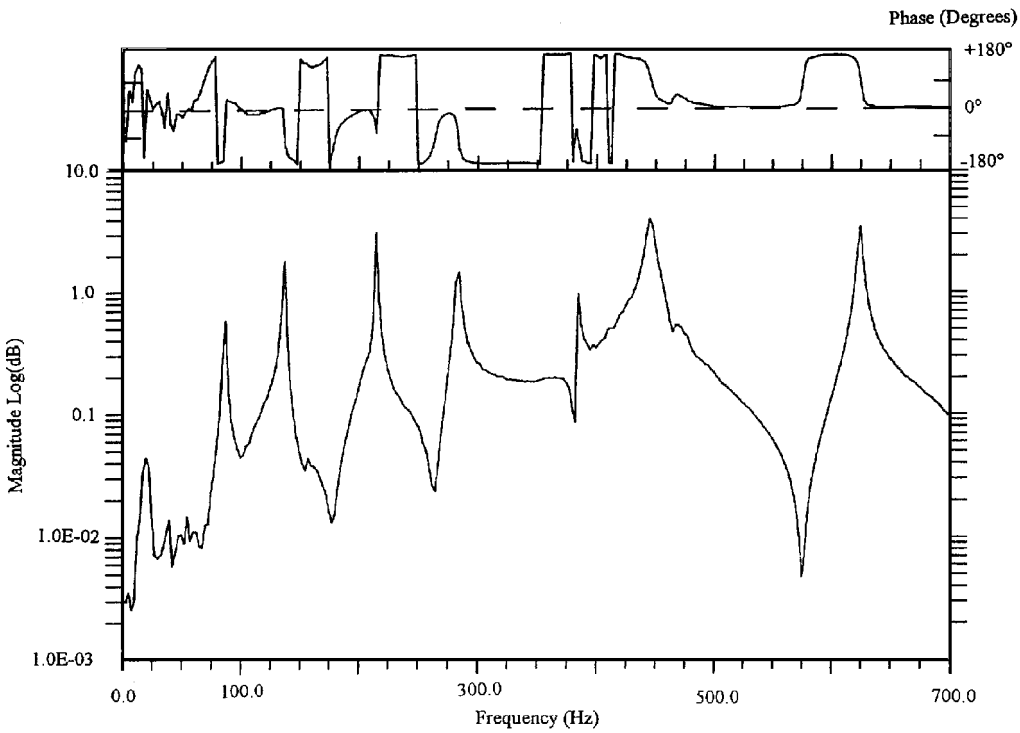

Fig. 8 Example of frequency response function taken from experimental modal analysis.

The discretized beam was manufactured by using Cytek 5245 epoxy prepregs with a T800 carbon fiber, the material properties of which are listed in Table 1. The beam was cured by a hot-press technique and postcure was also undertaken to minimize the amount of water absorbed in the beam. It was evident that, because of a small amount of resin leakage, the beam would have to be trimmed at one end. Consequently, the final element of the beam was 0.01 m instead of 0.02 m long. Although this affected the values of first bending and first torsional frequencies, the constraint of $\omega_{diff} \geq 750$ rad/s was still satisfied. A surface grid was then applied to the beam to facilitate modal analysis testing. A shock loading method of excitation was used with frequency data taken from an accelerometer mounted on one edge three-quarters of the way outboard from the root. Polynomial curve fitting was completed with the EMODAL[15] software package to obtain the natural frequencies and mode shapes of the beam. Figure 8 gives an example of frequency response function used in this process and illustrates the quality of the data obtained. For further details of the modal testing techniques used, see Ref. 16. Table 3 gives a comparison of the first eight natural frequencies obtained by the DSM and by experimental modal analysis. Percentage difference is calculated relative to the experimental results. As shown, the DSM gives frequencies that are within 11% of the experimental modal analysis results. In particular, the bending modes are predicted to an accuracy of within 4%. However, the discrepancies between the DSM calculated torsional frequencies and the experimental results do not follow a consistent pattern; the first torsional mode has a discrepancy of 7%, the second has a discrepancy of $\_11$%, and the third has a discrepancy of only $\_1$%. It is not completely understood why this is the case, but it may be due to a combination of the effects of neglecting shear deformation, warping stiffness, and rotary inertia in derivation of the dynamic stiffness matrix in Eq. (17). Furthermore, the DSM does not include any form of damping, either structural or aerodynamic, and thus the DSM frequency results should be higher than the experimental results, which are damped. Table 3 shows that this is the case only for the first three modes.

C. FEM Comparison

In addition to the modal analysis, the DSM was validated against a FEM model constructed with the commercial package ANSYS.[9] The model consisted of 312 eight-noded shell elements, which allowed for shear deformation. Each element had dimensions of 0.01×0.01 m. The resultant natural frequencies are given in Table 3. As shown, the differences between the FEM results and the experimental modal analysis are marginally greater (maximum of 13%), with the exception of mode 5, than the difference between the DSM and the experimental results. The FEM results, which were all fully converged, are consistently higher than the experimental results. To investigate this, a FEM model with a finer mesh (having 0.005×0.005 m elements) was examined. The frequencies obtained differed from those given in Table 3 by less than 0.5%, suggesting that the discrepancies may be for the follwing two reasons. First, the FEM model did not include the effect of structural and aerodynamic damping. Second, the FEM model did not account for the mass of the accelerometer.

Table 3 Comparison of natural frequencies obtained from experimental, DSM, and FEM modal analysis

Mode no.	Mode shape[a]	Experiment, Hz	FEM (% difference), Hz	DSM (% difference), Hz
1	1B	19.4	20.3 (+5)	19.9 (+3)
2	2B	86.7	91.7 (+6)	90.3 (+4)
3	1T	137.0	154.3 (+13)	146.0 (+7)
4	3B	215.3	217.8 (+1)	213.0 (−1)
5	2T	284.0	304.0 (+7)	252.8 (−11)
6	4B	384.8	394.3 (+2)	384.0 (0)
7	3T	445.4	494.5 (+11)	441.1 (−1)
8	5B	624.8	654.1 (+5)	611.4 (−2)

[a]B indicates a bending mode, and T indicates a torsional mode; e.g., 3B is the third bending mode.

Having investigated the effect of including a lumped mass at the accelerometer position within the DSM beam model, it was found that although the bending results were not affected (less than 0.5% difference), the torsional results were reduced by a maximum of 4% when an accelerometer was included in the model. Thus, if this effect had been taken into account with the FEM model, it is likely that the torsional results would have been closer to the experimentally obtained values.

Examination of the eight experimental, FEM, and DSM mode shapes corresponding to the results presented in Table 3 showed that each analysis method produced very similar mode shapes at the given frequencies.

Note that the computational run times for each analysis method differed greatly. The FEM modal analysis took approximately 420 s of CPU time on a SUN SPARC 10, whereas the equivalent modal analysis with the DSM took less than 3 s. The entire optimization process with the DSM took approximately 10 min.

IV. Concluding Remarks

Optimum design of nonuniform flat composite beams subject to frequency constraints has been considered. The associated natural frequencies have been calculated by using the DSM and have been validated by experimental modal analysis and commercial finite element software.

A generic composite layup has been optimized given a variety of frequency constraints specified in terms of the separation of first bending and first torsional natural frequencies. The optimizer was able to drastically reduce the mass of the beams by both minimizing the amount of 90- and 0-deg fibers within the structure and maximizing the effectiveness of +45- and −45-deg fibers. The resultant design for a frequency separation of 750 rad/s has been manufactured and subject to an experimental modal analysis, the results of which agree well with those predicted by the DSM.

Additional validation was provided by the FEM, the results of which compared well with the DSM frequencies and the experimental modal analysis. Given that the run time for the finite element calculations was of the order of 7 min (whereas the DSM took only a few seconds and uses a much simpler model—20 elements as opposed to 312), it is evident that the DSM is an extremely efficient and accurate method for modeling this type of problem.

Acknowledgments

The first author is supported by the Engineering and Physical Sciences Research Council under Studentship 94301807. The authors wish to express their sincere appreciation to J. R. Banerjee and S. Guo (City University) for permitting use of the dynamic stiffness method software in the optimization. They are also grateful to P. S. Keogh and J. Lee (University of Bath) for their helpful advice.

References

[1]Shirk, M. H., Hertz, T. J., and Weisshaar, T. A., "Aeroelastic Tailoring—Theory, Practice and Promise," *Journal of Aircraft*, Vol. 23, No. 1, 1986, pp. 6–18.

[2]Grandhi, R., "Structural Optimization with Frequency Constraints—A Review," *AIAA Journal*, Vol. 31, No. 12, 1993, pp. 2296–2303.

[3]Weisshaar, T. A., and Foist, B. L., "Vibration Tailoring of Advanced Composite Lifting Surfaces," *Journal of Aircraft*, Vol. 22, No. 2, 1985, pp. 141–147.

[4]Hollowell, S. J., and Dugundji, J., "Aeroelastic Flutter and Divergence of Stiffness Coupled, Graphite/Epoxy Cantilevered Plates," *Journal of Aircraft*, Vol. 21, No. 1, 1984, pp. 69–76.

[5]Georghiades, G. A., Guo, S. J., and Banerjee, J. R., "Flutter Analysis of Composite Wings Using an Exact Dynamic Stiffness Matrix Method," *Proceedings of the AIAA/ASME/ASCE/AHS/ASC 36th Structures, Structural Dynamics, and Materials Conference* (New Orleans, LA), AIAA, Washington, DC, 1995, pp. 3019–3027.

[6]Meirovitch, L., and Seitz, T. J., "Structural Modeling for Optimization of Low Aspect Ratio Composite Wings," *Journal of Aircraft*, Vol. 32, No. 5, 1995, pp. 1114–1123.

[7]Grandhi, R. V., Bharatram, G., and Venkayya, V. B., "Optimum Design of Plate Structures with Multiple Frequency Constraints," *Structural Optimization*, Vol. 5, Nos. 1–2, 1992, pp. 100–107.

[8]Butler, R., and Banerjee, J. R., "Optimum Design of Bending-Torsion Coupled Beams with Frequency or Aeroelastic Constraints," *Computers and Structures*, Vol. 60, No. 5, 1996, pp. 715–724.

[9]Anon., "ANSYS User's Manual," Version 5.0, Swanson Analysis Systems, Houston, TX, 1992.

[10]Tsai, W. S., and Hahn, T. H., *Introduction to Composite Materials*, Technomic, Westport, CT, 1980.

[11]Datoo, H. M., *Mechanics of Fibrous Composites*, Elsevier, Essex, England, UK, 1991.

[12]Banerjee, J. R., and Williams, F. W., "Free Vibration of Composite Beams—An Exact Method Using Symbolic Computation," *Journal of Aircraft*, Vol. 32, No. 3, 1995, pp. 636–642.

[13]Wittrick, W. H., and Williams, F. W., "A General Algorithm for Computing Natural Frequencies of Elastic Structures," *Quarterly Journal of Mechanics and Applied Mathematics*, Vol. 24, Pt. 3, 1971, pp. 263–284.

[14]Anon., "DOT Design Optimization Tools Users Manual," VMA Engineering, Goleta, CA, 1993.

[15]Anon., "EMODAL–PC Instruction Manual," ENTEK Scientific, Cincinnati, OH, 1988.

[16]Ewins, D. J., "Modal Testing: Theory and Practice," *Research Studies*, Taunton, England, UK, Jan. 1995, Chaps. 3, 4.

R. K. Kapania
Associate Editor